actuators

MDPI

Article

3-Bit Digital-to-Analog Converter with Mechanical Amplifier for Binary Encoded Large Displacements

Lisa Schmitt *, Philip Schmitt and Martin Hoffmann *

Faculty of Electrical Engineering and Information Technology, Ruhr-University Bochum (RUB), 44801 Bochum, Germany; philip.schmitt@rub.de

* Correspondence: lisa.schmitt-mst@rub.de (L.S.); martin.hoffmann-mst@rub.de (M.H.)

Abstract: We present the design, fabrication, and characterization of a MEMS-based 3-bit Digital-to-Analog Converter (DAC) that allows the generation of large displacements. The DAC consists of electrostatic bending-plate actuators that are connected to a mechanical amplifier (mechAMP), enabling the amplification of the DAC output displacement. Based on a parallel binary-encoded voltage signal, the output displacement of the system can be controlled in an arbitrary order. Considering the system design, we present a simplified analytic model, which was confirmed by FE simulation results. The fabricated systems showed a total stroke of approx. 149.5 ± 0.3 µm and a linear stepwise displacement of 3 bit correlated to $2^3 \triangleq$ eight defined positions at a control voltage of 60 V. The minimum switching time between two input binary states is 0.1 ms. We present the experimental characterization of the system and the DAC and derive the influence of the mechAMP on the functionality of the DAC. Furthermore, the resonant behavior and the switching speed of the system are analyzed. By changing the electrode activation sequence, 27 defined positions are achieved upgrading the 3-bit systems into a 3-tri-state (3^3) system.

Keywords: digital-to-analog converter; DAC; large displacements; electrostatic bending-plate actuator; mechanical amplifier; mechAMP; 3-tri-state system; dicing-free SOI-technology; MEMS

Citation: Schmitt, L.; Schmitt, P.; Hoffmann, M. 3-Bit Digital-to-Analog Converter with Mechanical Amplifier for Binary Encoded Large Displacements. *Actuators* **2021**, *10*, 182. https://doi.org/10.3390/act10080182

Academic Editors: Manfred Kohl, Stefan Seelecke and Ulrike Wallrabe

Received: 30 June 2021
Accepted: 31 July 2021
Published: 4 August 2021

1. Introduction

The presented cooperative multistage multi-stable actuator system with large stroke was motivated by terahertz (THz) applications where a free-space true-time delay is required. Usually, the true-time delay is subdivided in binary fractions of the wavelength. Mostly, MEMS-based reflect arrays for beam steering applications are driven by out-of-plane actuation [1], but this article focusses on an in-plane single-reflector system with a large displacement. The single in-plane chips are intended to be stacked together after fabrication to realize the mechanical beam steering in the THz range [2,3].

A digital actuator system would be a perfect solution to realize the in-plane discretized large throw. In order to avoid complex driving electronics, a micro-electromechanical digital-to-analog converter (M-DAC) based on cascaded actuators directly addressed by the digital signal is presented. A mechanical DAC converts an electrical binary code into a proportional output displacement [4]. These DACs consist of n electrostatic actuators reaching a finite number of 2^n positions inherent to the actuators. By adding more actuators, the positioning performance tends to approach the positioning performance of continuous systems [4]. The M-DACs allow accurate, stable and repeatable displacements without extensive feedback control circuits or strict control requests [4]. In contrast to actuators driven by analog voltages, such systems do not need a careful position control including sensing.

Apart from beam steering applications, M-DACs can be used for open-loop operation [5] with high-position resolution and for optical surface profiling [6]. Yeh et al. [7] proposed a thermal actuation for a 3-bit maximum stroke of 5.8 µm at 5 V control voltage

(Table 1). Liu et al. [8] presented a 4-bit weighted stiffness micro-electromechanical DAC with a maximum stroke of 3.75 µm and a control voltage of 5 V. Pandiyan et al. [9] suggested two different concepts based on a bent beam electrothermal compliant actuator as a single mechanical bit reaching maximum strokes of 44 µm and 45 µm at 5 V. As thermal actuators induce heating of the entire microsystem, these actuators are not practicable for applications requiring high precision positioning and quick response times. The drawback of electrostatic actuators is the comparable high voltage required for a large displacement. However, the works of Toshiyoshi et al. [10] and Sarajic et al. [4,11] showed that a strategic optimization of the system setup can lower the control voltage and increase the total stroke. By using comb-drive actuators, Toshiyoshi et al. and Sarajic et al. reached binary encoded displacements of 5.8 µm at 150 V and 8.57 µm at 45 V, respectively.

Table 1. Comparison of digital-to-analog converters from the literature.

Ref.	Actuation	No. of Bits	Maximum Stroke	Voltage
[7]	thermal	3	5.8 µm	5 V
[8]	electrothermal compliant	4	3.75 µm	5 V
[9]	electrothermal compliant	4	44 µm/45 µm	5 V/5 V
[10]	electrostatic (comb-drive)	4	5.8 µm	150 V
[4,11]	electrostatic (comb-drive)	12	8.57 µm	45 V
this work	electrostatic (bending-plate)	3/3-tri-states	DAC + mechAMP: 149.5 µm only DAC: 21.4 µm	60 V/75 V

In this paper, we present an in-plane 3-bit DAC consisting of cascaded flexible electrostatic bending-plate actuators for large displacement applications at low voltage. We report the combination of a DAC with a mechanical amplifier (mechAMP) [12] to generate large strokes of up to 149.5 µm at 60 V, including the control of $2^3 \triangleq 8$ discrete positions. By changing the electrode activation sequence, we can approach three states with every bit, thus enlarging the system application field to a 3-tri-state system driving $3^3 \triangleq 27$ discrete defined positions.

In Section 2 the single system components and the system concept are presented. Based on this, we derive the analytic transfer function and design the system supported by FE simulation. Section 3 shows the SOI fabrication process. Section 4 presents the experimental setup and the characterization results. We characterize the function of the DAC, of the mechAMP and of the combined system; the switching speed; the resonant behavior and the expansion of the 3-bit system to a 3-tri-state system. The main achievements of this work are summarized in Section 5.

2. Concept

2.1. System Components

The displacement of the system is generated by combining high-throw electrostatic bending-plate actuators [2,13]. These actuators are illustrated in Figure 1a and consist of long, nonrigid cantilevers and electrodes with low stiffness.

The cantilever of the fixed actuator (f3) is clamped. The cantilever of the moving actuator (m2) is directly linked to a linear rotor guided and fixed by a flexible spring. The electrodes (m1, f1) face each other at a distance $x_{\text{electrode}}$. When applying a voltage between the electrodes, the cantilevers and electrodes bend down as soon as the electric force attracting the electrodes exceeds the mechanical force of the cantilevers, electrodes and the spring. At low voltage, the tips of the electrodes (m1, f1) begin to approach. With increasing voltage, the pull-in is completed, as illustrated in Figure 1b.

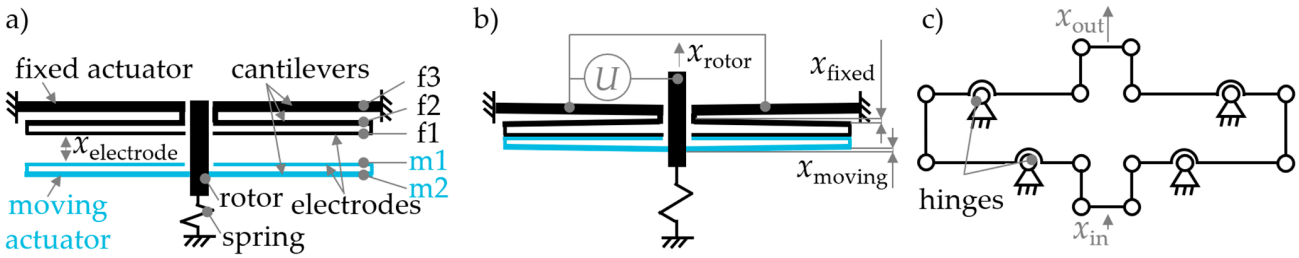

Figure 1. (**a**) Setup of a high-throw electrostatic bending-plate actuator. (**b**) Bending-plate actuator traveling the distance x_{rotor} after the application of a voltage. (**c**) Setup of the mechAMP converting a small input displacement x_{in} into a large output displacement x_{out}. (drawings not to scale).

The distance covered by the linear rotor x_{rotor} corresponds to the electrode gap $x_{electrode}$ before pull-in, deducting the deflection of the fixed and the moving actuators x_{moving} and x_{fixed} (Figure 1b), which yields:

$$x_{rotor} = x_{electrode} - (x_{fixed} + x_{moving}) \quad (1)$$

The displacement of the electrostatic actuators is amplified by a passive micromechanical amplifier (mechAMP) [12], as shown in Figure 1c. It consists of cascaded levers connected by flexure hinges. The amplification ratio $A_{mechAMP}$ is designed by adjusting the hinges to convert a small input displacement x_{in} into a large output displacement x_{out}. The input stiffness of the mechAMP is defined by the length of the beams and by the thickness and the position of the flexure hinges.

2.2. System Function

The system (Figure 2a) consists of two components: a mechAMP and a 3-bit DAC driven by multiple electrostatic actuators. The binary encoded discrete displacement (small stroke but high force) generated by the DAC x_{DAC} is amplified by the mechAMP, resulting in a large and still binary-encoded discrete total system displacement x_{system}.

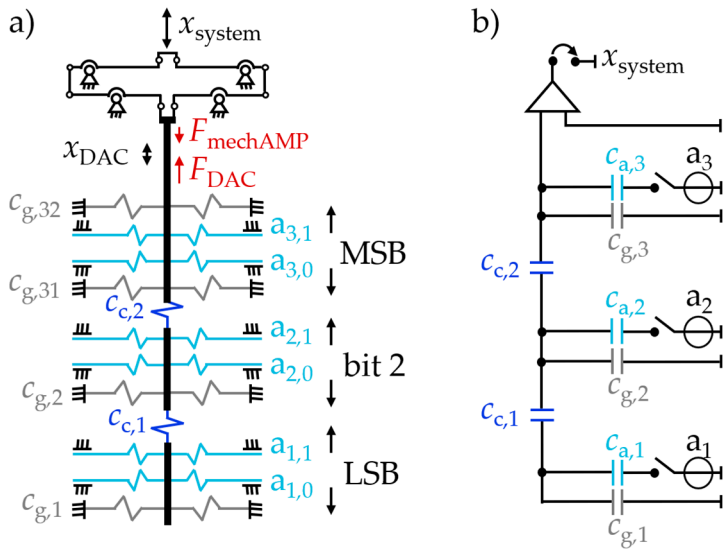

Figure 2. (**a**) Structure of the system: the binary encoded discrete displacement of the DAC x_{DAC} is amplified by the mechAMP, resulting in a large and still binary-encoded discrete system displacement x_{system}, (**b**) corresponding electrical network model. (drawings not to scale).

The 3-bit DAC (Figure 2a) consists of multiple electrostatic actuators a_i with a stiffness $c_{a,i}$. Each bit has actuators $a_{i,0}$ that can travel downwards (0-direction) and actuators $a_{i,1}$ that can travel upwards (1-direction). The electrode gaps $x_{electrode,i}$ are identical for each actuator. The bits are connected by springs $c_{c,i}$. Sinusoidal guiding springs $c_{g,i}$ connect

the system to the substrate. Bit 3, the most significant bit (MSB), is connected to the mechAMP. To increase the stability of the mechAMP and the MSB, the MSB is connected to the substrate by two guiding springs, $c_{g,32}$ and $c_{g,31}$, whereas the other two bits feature only one guiding spring, $c_{g,1}$ and $c_{g,2}$, respectively.

Figure 3 exemplarily shows the different states of the DAC. Each bit is either shifted upwards or downwards. When all downwards-actuators ($a_{i,0}$) are displaced, the system is in position 000 (Figure 3a). The system obtains the next logical position (001) when the upward actuators of the least significant bit (LSB, bit 1) $a_{1,1}$ are activated and the downwards actuators $a_{1,0}$ are deactivated at the same time (Figure 3b). When all upwards actuators ($a_{i,1}$) are displaced, the system is in position 111 (Figure 3c).

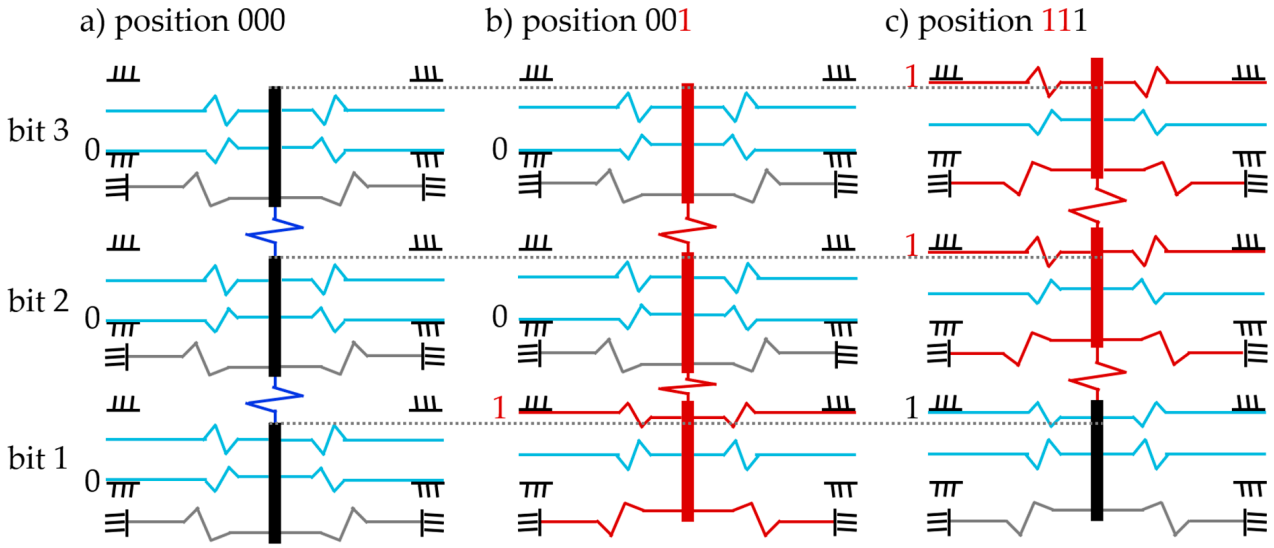

Figure 3. DAC in (**a**) the 000 position by activating the $a_{i,0}$ actuators; (**b**) the 001 position by activating the $a_{1,1}$, $a_{2,0}$ and $a_{3,0}$ actuators and (**c**) the 111 position by activating the $a_{i,1}$ actuators. (drawings not to scale).

In an electrical network model (Figure 2b), the actuators are modeled as potential sources, and the mechanical springs are associated with the capacitors. The network model allows the derivation of the analytic transfer function (2) for the DAC [2]:

$$\begin{pmatrix} c_a + c_g + c_c & -c_c & 0 \\ -c_c & c_a + c_g + 2c_c & -c_c \\ 0 & -c_c & c_a + c_g + c_c \end{pmatrix} \cdot \begin{pmatrix} x_{rotor,1} \\ x_{rotor,2} \\ x_{rotor,3} \end{pmatrix} = \begin{pmatrix} F_{a,1} \\ F_{a,2} \\ F_{a,3} \end{pmatrix} \quad (2)$$

Equation (2) is valid as long as each bit features a displacement either corresponding to a 0- or to 1-direction ($x_{a,1,0} \neq x_{a,1,1}$, $x_{a,2,0} \neq x_{a,2,1}$ and $x_{a,3,0} \neq x_{a,3,1}$), assuming each actuator has the same stiffness ($c_{a,1} = c_{a,2} = c_{a,3}$) and travels the same distance ($x_{rotor,1} = x_{rotor,2} = x_{rotor,3}$). All connecting springs ($c_{c,1} = c_{c,2} = c_{c,3}$), as well as all guiding springs ($c_{g,1} = c_{g,2} = c_{g,3}$), have the same stiffness [2].

As illustrated in Figure 2a, the mechanical force of the DAC F_{DAC} must overcome the stiffness of the mechAMP $F_{mechAMP}$. For $F_{DAC} >> F_{mechAMP}$, the system displacement yields:

$$x_{system} = x_{DAC} \cdot A_{\ mechAMP} \quad (3)$$

2.3. System Modeling and Simulation

The function of the system and its components is verified by solid-state mechanic and electrostatic finite-element (FE) simulations carried out in COMSOL Multiphysics. The optimization is focused on a maximum stroke and a linear stepwise displacement.

A single electrostatic actuator is analyzed using 2D electrostatic stationery and time-dependent FE simulations based on the setup shown in Figure 4. The flexible electrodes

are clamped at each end. The voltage between the electrodes is systematically increased. During simulation, a moving mesh is used. Spacers defined as contact pairs allow a steady simulation. These semicircular-formed spacers are adopted for the fabrication of the electrostatic actuators, as they minimize the contact area of the electrodes and, therefore, also the risk of a short circuit during experimental characterization. The simulation of the single actuator shows a pull-in voltage of the tips between 20 V and 30 V.

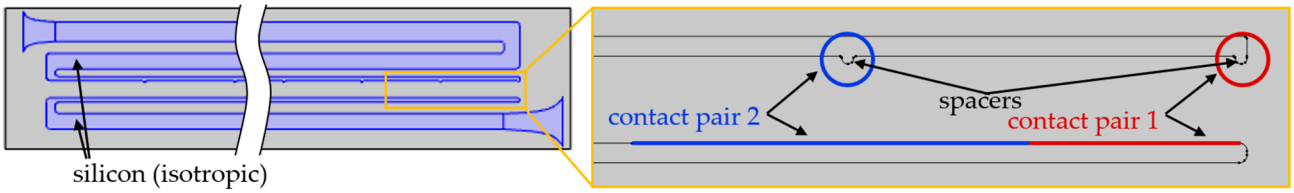

Figure 4. Simulation setup of a single actuator by COMSOL Multiphysics: a voltage is systematically increased between the electrodes, and the spacers defined as contact pairs allow a steady simulation.

As explained in Section 2.1, the cantilevers of the bending-plate actuators bend when a sufficiently high voltage is applied. To achieve a high displacement of the rotor x_{rotor} (Equation (1)), the stiffness of the fixed actuator must exceed the stiffness of the moving system. Therefore, the cantilever stiffness has to be sufficiently high to overcome the stiffness of the guiding and connecting springs. However, a higher stiffness of the cantilevers results in a higher pull-in voltage. To optimally balance the opposing requirements for low pull-in voltage and large displacement, multiple actuators connected in a parallel configuration are used. In this arrangement, the single actuator features a low pull-in voltage due to its low stiffness, but the total stiffness is increased by the connection of multiple actuators. Figure 5 shows such an actuator consisting of twelve single identical high-throw bending-plate actuators for each direction. The electrodes of the actuators have a thickness $t_{a,m1/f1}$ = 5 µm and length $L_{a,m1/f1}$ = 2210 µm. The lengths of the cantilevers amount to $L_{a,f3}$ = 2235 µm and $L_{a,m2}$ = 2265 µm, the thickness is $t_{a,f3/m2}$ = 25 µm and $t_{a,f2}$ = 20 µm.

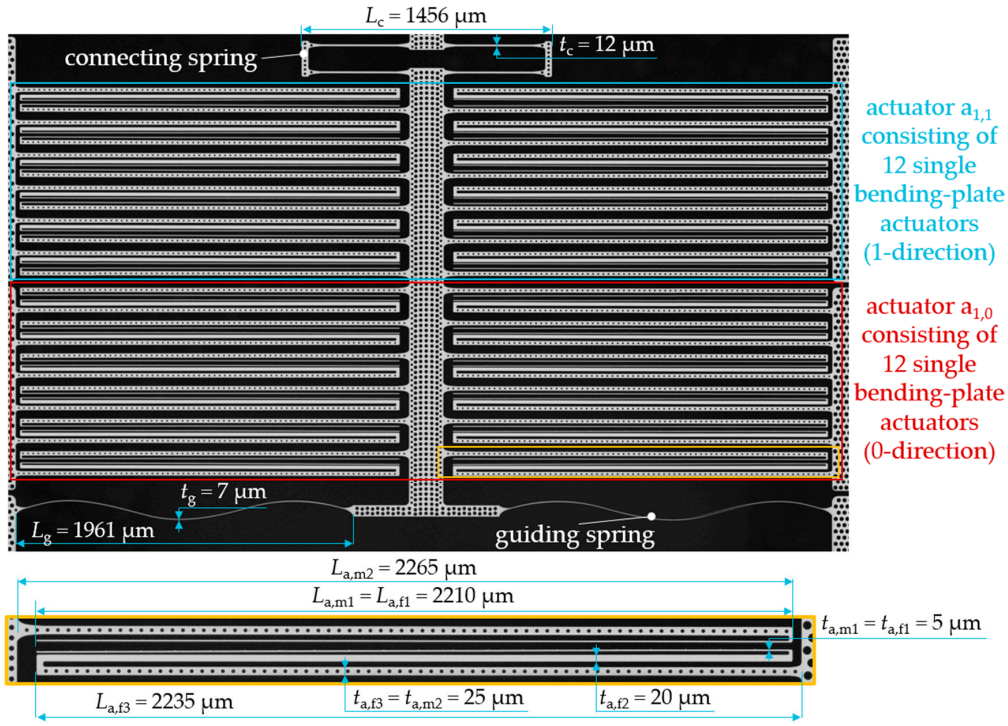

Figure 5. Bit 1 fixed by guiding springs and connected to bit 2 by a connecting spring. Each actuator, $a_{1,0}$ and $a_{1,1}$, consists of 12 single bending-plate actuators (stiching microscope image).

The guiding springs connect the DAC to the substrate and prevent an in-plane rotation. The sinusoidal guiding springs (Figure 5) are well-suited here, as they feature a very low stiffness in the deflection direction, lowering the pull-in voltage and, therefore, increasing the displacement of the actuators [14]. However, in off-axis directions, these springs show a high stiffness ensuring a purely translational guiding of the system [14]. The guiding springs feature the thickness t_g = 7 µm and the length L_g = 1.961 µm. The connecting springs (Figure 5) combine the single bits and feature a high stiffness to guarantee the transmission of the actuator displacement to the system output. The minimum thickness of the connecting springs t_c amounts to 12 µm, and the length L_c is 1456 µm.

For the mechanical amplification of the DAC output displacement, we use the two different concepts of displacement amplification presented in Figure 6. The function principle of mechAMP+ shown in Figure 6a is identical to the version presented in Figure 1c. The mechAMP+ features four hinges with a minimum thickness t_{hinge} = 3 µm and directly converts the small input displacement x_{in} in a large output displacement x_{out}. Instead of hinges, the mechAMP– in Figure 6b is guided by a triangular spring [14] at the output. The spring features 26 beams with an inclination angle $\alpha = 60°$ and has a thickness t_{spring} of 5 µm and a length L_{spring} of 2952 µm. This spring provides additional stability for the connection of the mechAMP to the substrate. Therefore, the mechAMP– does not only convert the small input displacement x_{in} into a large output displacement x_{out}, it also inverts the input signal. As illustrated in Figure 6b, a positive input displacement results in a negative output displacement and vice versa.

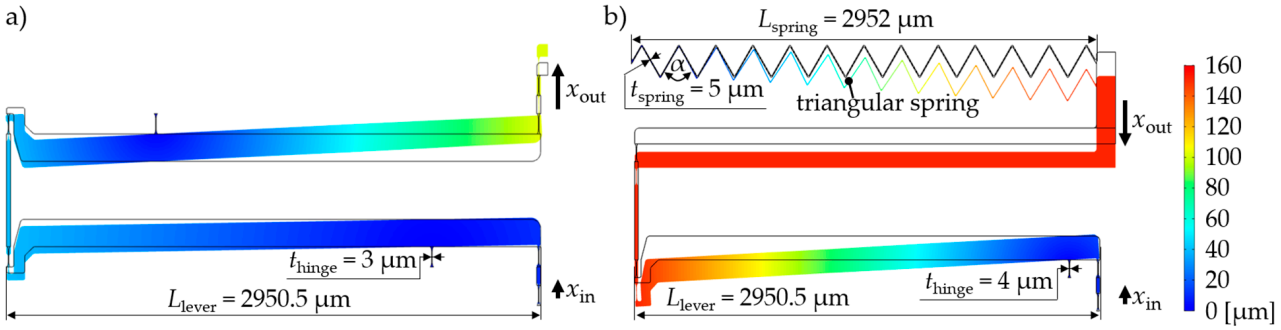

Figure 6. MechAMPs displaced the distance x_{in} = 10 µm by the COMSOL Multiphysics simulation. Due to the symmetric setup, only the left hand side of the mechAMPs is shown. (**a**) MechAMP+ amplifies the input displacement x_{in} in a large output displacement x_{out}, and (**b**) MechAMP– amplifies and inverts the input displacement x_{in} in a large and inverse output displacement x_{out}.

Based on the presented considerations, we model two systems consisting of different mechAMPs and DACs, shown in Table 2. The modeling results refer to an electrode displacement of 10 µm. The sinusoidal guiding springs feature a stiffness of c_g = 0.7 N/m, the connecting springs of c_c = 128 N/m and the actuators of c_a = 92 N/m. DAC 1 features an additional spring connecting the LSB to the substrate (Figure 7i).

The modeled systems show maximum strokes $x_{system,max}$ of 143.7 µm and 167.1 µm, respectively. The step sizes amount to 20.5 ± 6.7 µm and 23.9 ± 3.1 µm, respectively. DAC 1 and DAC 2 achieve maximum strokes of $x_{DAC1,max}$ = 17.8 µm and $x_{DAC2,max}$ = 19.8 µm, respectively. MechAMP+ features an amplification ratio of 10.3 with an input stiffness of 44.7 µN. MechAMP+ lowers the maximum stroke of DAC 1 to 14.0 µm. MechAMP– has a higher amplification ratio of 15.1 but, also, a higher input stiffness of 127.4 µN, lowering the maximum stroke of DAC 2 to 11.1 µm. The size of system 1 amounts to 10,500 × 5980 µm^2, and the chip size amounts to 15,165 × 10,930 µm^2 (Table 2 and Figure 7i).

Table 2. Simulated DACs, mechAMPs and systems at a displacement of $x_{electrode}$ = 10 µm.

		System 1 (Figure 7i)	System 2
DAC	*version*	*DAC 1*	*DAC 2*
	$x_{DAC,max}$	17.8 µm	19.8 µm
	step size	2.5 ± 0.8 µm	2.8 ± 0.4 µm
mechAMP	*version*	*mechAMP+*	*mechAMP–*
	amplification ratio	10.3	15.1
	input stiffness	44.7 µN	127.4 µN
DAC combined to mechAMP	$x_{DAC,max}$	14.0 µm	11.1 µm
	step size	2.0 ± 0.7 µm	1.6 ± 0.2 µm
system	$x_{system,max}$	143.7 µm	167.1 µm
	step size	20.5 ± 6.7 µm	23.9 ± 3.1 µm
	system size	10,500 × 5980 µm^2	11,080 × 6144 µm^2
	chip size	15,165 × 10,930 µm^2	15,707 × 10,930 µm^2

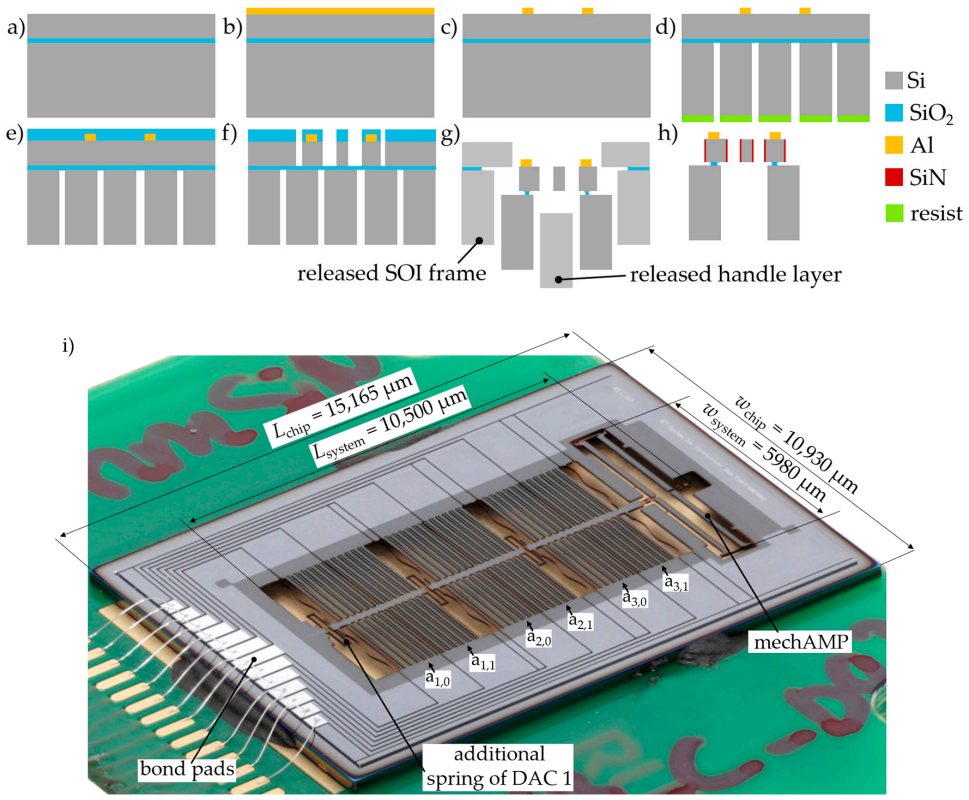

Figure 7. Fabrication process (drawings not to scale): (**a**) SOI Wafer, (**b**) deposition of the aluminum layer, (**c**) etching of the bond pads, (**d**) deep etching of the handle layer, (**e**) PECVD of 400-nm SiO_2, (**f**) deep etching of the device layer, (**g**) HF vapor etching, (**h**) deposition of 400-nm SiN and (**i**) fabricated chip fixed and wire-bonded to a circuit board (stacked device photo).

3. Fabrication

The microsystems are fabricated on (100)-oriented Silicon-on-Insulator (SOI) wafers (Figure 7a) with a 300-µm-thick handle layer and a 50-µm-device layer. To minimize the risk of a pull-in between the electrostatic actuators and the handle layer and to prevent a parasitic out-of-plane motion during electronic activation, the chips are fabricated by a dicing-free process [15,16]. This process separates the chips from each other, making the

mechanical sawing process obsolete and, also, allows the removal of the handle layer from the backside of the electrostatic actuators during hydrofluoric (HF) vapor etch release.

First, a 100-nm aluminum layer is deposited on the device layer by evaporation (Figure 7b), and the bond pads are patterned by wet chemical etching (Figure 7c). Then, the resist (AZ MIR 701 29 cp) is spin-coated with 1000 rpm onto the handle layer as a mask during deep etching. For deep etching, an alternating SF_6/C_4F_8-based deep reactive ion etching process (DRIE) is used (Figure 7d). After O_2 plasma, a 400-nm SiO_2 layer is deposited by a plasma-enhanced chemical vapor deposition (PECVD) process (Figure 7e). The SiO_2 layer is used as a hard mask for the patterning of the structures into the device layer. Then, the structures are patterned and deep-etched (Figure 7f). HF vapor etching releases the moveable structures (Figure 7g). Then, the electrodes are isolated by depositing 400-nm silicon nitride (SiN) with a low-stress PECVD process (Figure 7h). During this process, the chips are flipped to reduce the spacing between the electrodes and the carrying wafer, which also prevents a coating of the bond pads with isolating SiN. In the final step, the chips are fixed to a circuit board and wire-bonded (Figure 7i).

4. System Characterization Results

4.1. Experiment and Characterization Setup

The systems are characterized using a highspeed camera system (Keyence VW-600C) and a voltage source (EA- Electro-Automatic PS-3200-02 C). The characterization setup is presented in Figure 8.

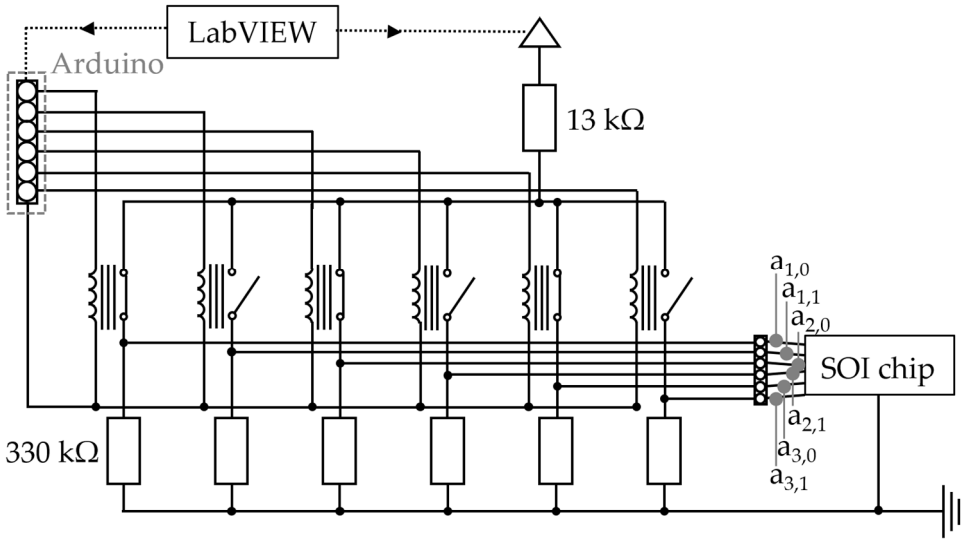

Figure 8. A LabVIEW program controls the voltage source, with an Arduino activating the relays in an arbitrary order and as a function of time. The relays are connected to the actuators of the SOI chip. Here, the relays are exemplarily activated to drive the 000 position.

The LabVIEW program controls the voltage source and an Arduino that drives the single bits of the microsystem by activating and deactivating the relays on a circuit board in an arbitrary order and as a function of time. The relays are connected to the actuators on the SOI chip. Pull-down resistors of 330 kΩ are connected between the electrostatic actuators and the ground potential to enable a quick discharge of the electrodes. The 13-kΩ resistor limits the current flow to prevent an eventual breakthrough of the SiN isolation at the electrodes. For the actuation of the electrostatic actuators, a DC voltage is used.

Based on the videos recorded by the highspeed camera during the activation of the DAC, the displacement of the system and its components is analyzed. Due to the very high aspect ratio (length vs. displacement) and due to the symmetric setup of the system, the videos show either the middle, the left or the right side of the system. To analyze the videos, the software *Tracker* allows marking of the strategic tracking points.

4.2. Characterization of the System

4.2.1. System Function Testing

Figure 9 illustrates the operation of the system. Depending on the activated actuators, the mechAMP and, with it, the output of the system is displaced from maximum (111 position) to the minimum (000 position) displacement.

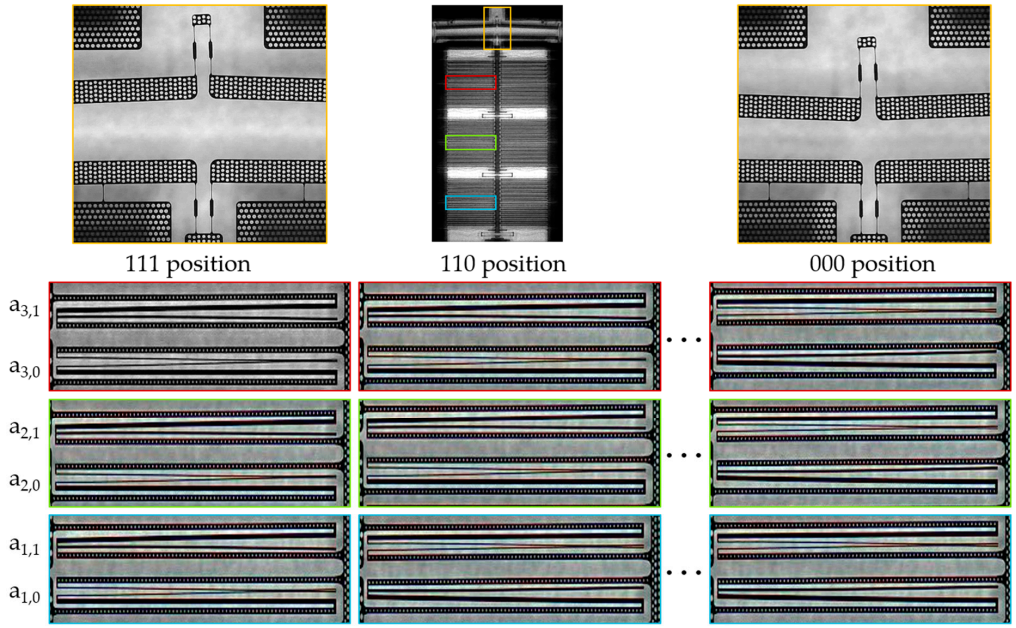

Figure 9. (**Top**) Middle: system 1, left: mechAMP+ in the 111 position, right: mechAMP+ in the 000 position. (**Bottom**) Left: actuators in the 111 position, middle: actuators in the 110 position, right: actuators in the 000 position. Due to the high aspect ratio, the length of the actuators is compressed by 50%.

4.2.2. Characterization of the DAC

In a first characterization step, the pull-in voltage of the single bits in relation to the driven position is analyzed in Figure 10. Each position is approached in logical order from the 111 to 000 position. Starting with an initial voltage of 30 V, the voltage is increased in 5 V-steps, until a pull-in of all actuators of each single bit is achieved.

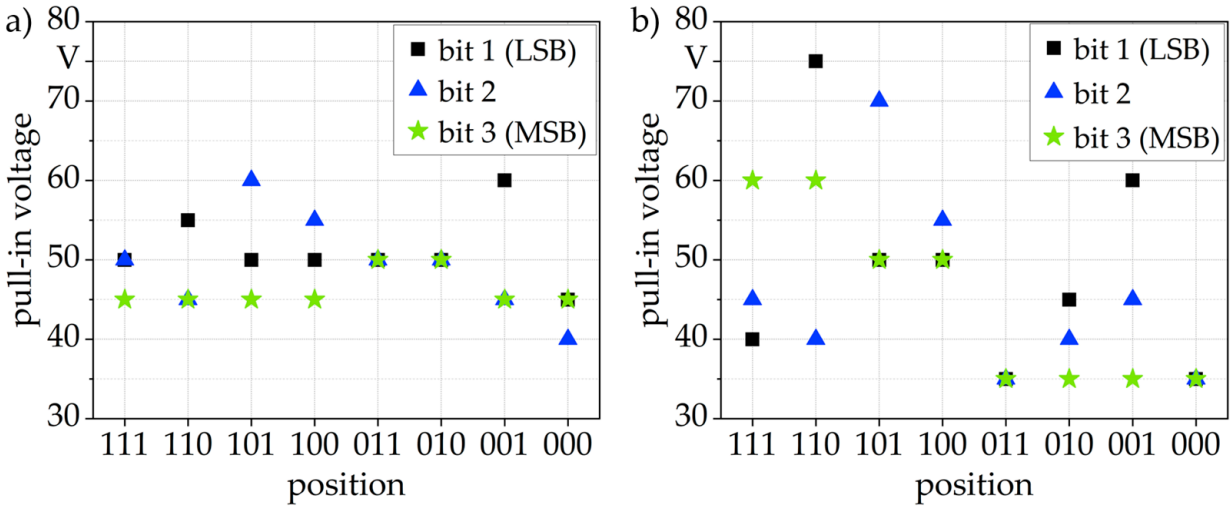

Figure 10. Pull-in voltage of the single bits is dependent on the driven position for (**a**) system 1 and (**b**) system 2. During the experiment, the voltage increased in 5 V-steps, until a pull-in of all the actuators of each single bit was achieved.

Bit 2 of system 1 (Figure 10a) shows the lowest pull-in voltage of 40 V at the 000 position. As bit 1 and bit 3 pull in at 45 V, the pull-in voltage at the 000 position amounts to 45 V. The 001 and 101 positions have the highest pull-in voltage of 60 V. Therefore, a control voltage of 60 V is chosen for system 1. Consequently, the control voltage of system 2 (Figure 10b) amounts to 75 V. The high input stiffness of mechAMP– can be considered as the cause for the higher control voltage of system 2.

At first glance, the derived control voltage of the system appears very high. In order to classify this result, a linear relationship between the displacement and voltage is assumed. System 1 reaches a total displacement of 150 µm at 60 V, which corresponds to 2.5 µm per 1 V. The electrostatic comb-drive DACs [4,10,11] presented in Table 1 reached a displacement of approx. 0.04 µm and 0.2 µm per 1 V, respectively. The electrostatic parallel-plate actuator presented in reference [13] reached a displacement of 65 µm at 30 V, which corresponds to 2.2 µm per 1 V. Therefore, in relation to the achieved displacement, the voltage of the presented system is rather low.

During the experimental characterization of the DAC, stiction issues appeared at low voltages. Thus, at the selected control voltage, no stiction issues were observed in the further experiments. Additionally, when varying the switching speed in the range from 2 s to 0.1 milliseconds, no stiction issues were observed.

Figure 10 shows that the pull-in voltage of the electrostatic actuators depends on the system, the bit and on the driven position. For system 1 (Figure 10a), the MSB usually exhibited a lower pull-in voltage than the LSB and bit 2. The stiffness of the additional connecting spring (Figure 7i) that the LSB was connected to was higher than the input stiffness of the mechAMP+ that the MSB was connected to. Therefore, the MSB had to overcome a lower mechanical stiffness than the LSB and had a lower pull-in voltage. Apart from positions 111 and 000, bit 2 always displaces in the opposite direction either of the MSB or of the LSB, which increased the pull-in the voltage of bit 2. At the 000 and 111 positions, the actuators tended to show a low pull-in voltage, so that the displacement of all actuators in the same direction seemed to support a low pull-in voltage.

The displacement of the actuators depending on the driven position was analyzed experimentally, as presented in Figures 11 and 12

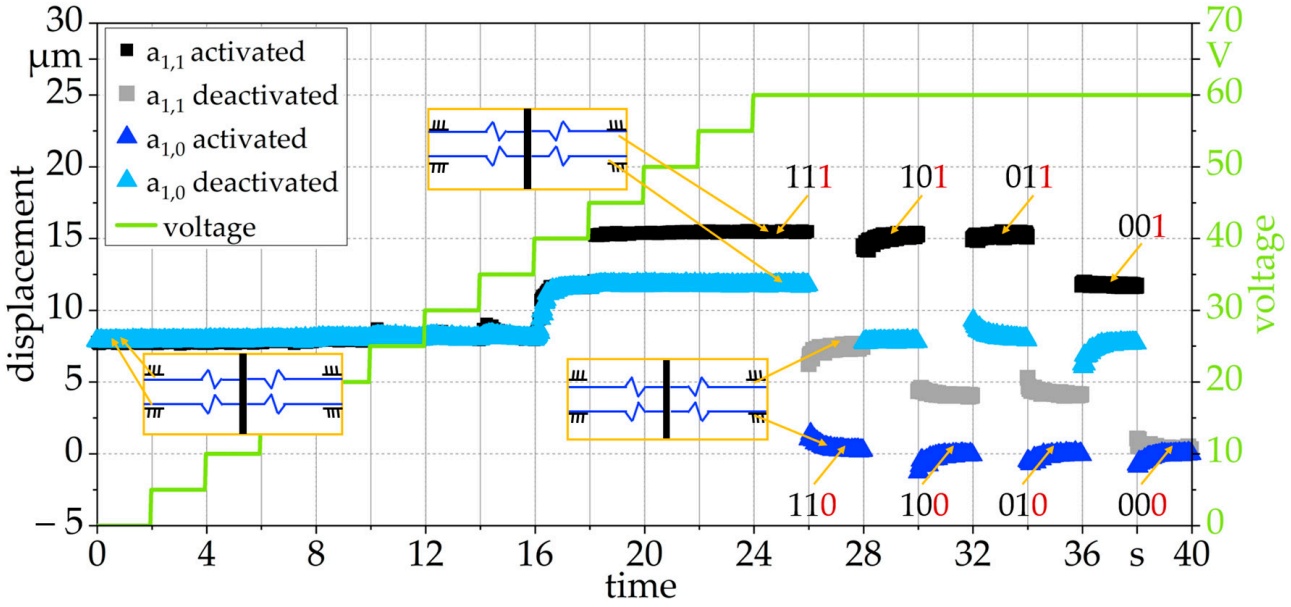

Figure 11. Displacement of the actuators $a_{1,1}$ and $a_{1,0}$ of the LSB of system. First, the voltage is increased from 0 V to 60 V in 5 V-steps every 2 s. At 60 V, the voltage remains stable while switching every 2 s in logical order from the 111 to 000 position.

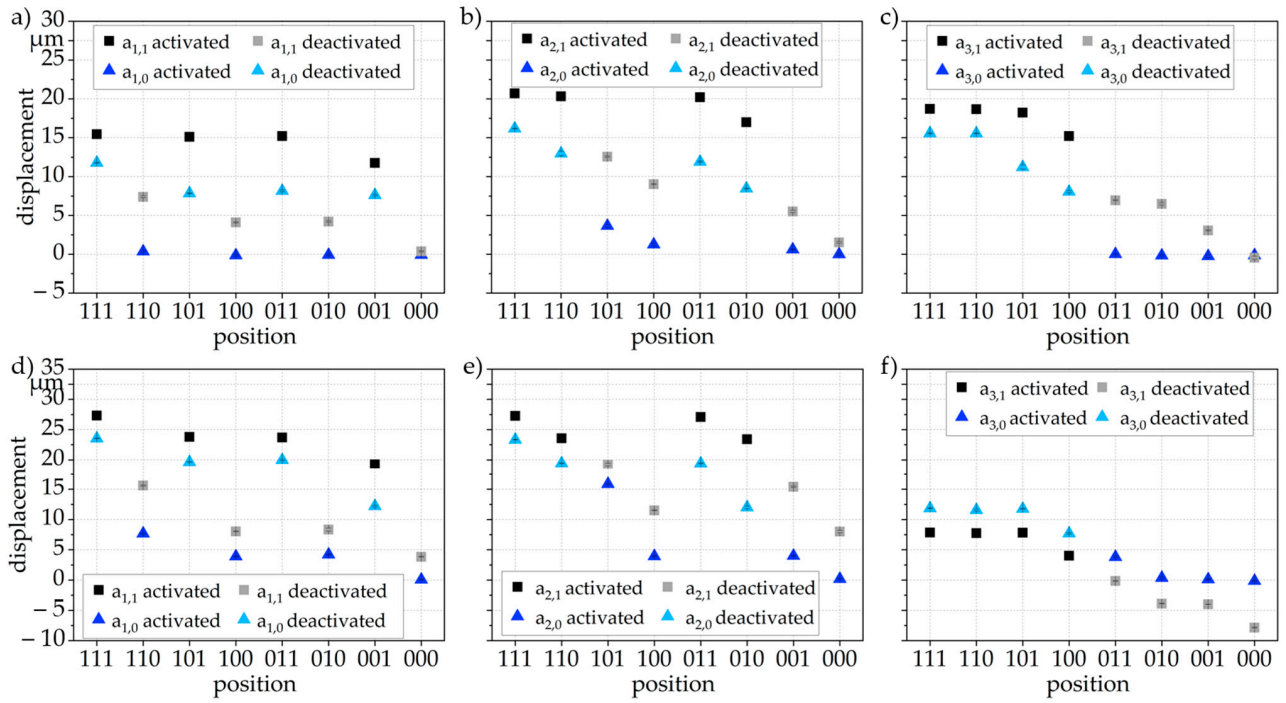

Figure 12. Experimental average actuator displacement of the single bits; each experiment was repeated three times. The experimental conditions correspond to the description in Figure 11. (**a**) Bit 1, (**b**) bit 2 and (**c**) bit 3 of system 1 at 60 V and (**d**) bit 1, (**e**) bit 2 and (**f**) bit 3 of system 2 at 75 V.

In Figure 11, we exemplarily show the time-dependent displacement of the actuators of the LSB. To reach the starting 111 position, the voltage is increased in 5-V-steps every 2 s. At the selected control voltage, the positions are switched in 2-s intervals in logical order from the 111 to 000 position. During the increase of the voltage, clearly visible displacements start at 35 V for the activated actuators $a_{1,1}$ and the deactivated actuators $a_{1,0}$. The displacement of the deactivated actuators is a passive displacement caused by the displacement of the activated actuators. Switching from the 111 to 110 position, the $a_{1,0}$ actuators are activated and the $a_{1,1}$ actuators deactivated.

Based on the experiment presented in Figure 11, the average displacement of each bit is shown in Figure 12. The DAC of system 1 (Figure 12a–c) shows a quite stable behavior. For each bit, the activated actuators shift to approx. the same displacement. The deactivated actuators follow the displacement of all the activated actuators in the microsystem. The shift of the deactivated actuators is less than the shift of the activated actuators.

For system 2, the displacement of the deactivated actuators of bit 3 (Figure 12f) exceeds the displacement of the activated actuators. The very low shift of the MSB is possibly due to the high input stiffness of mechAMP– that bit 3 is connected to, resulting in a less-stable displacement of bit 1 and bit 2, as shown in Figure 12d,e.

4.2.3. Characterization of the Combined DAC and mechAMP

To characterize the system, the single actuators are activated in logical order from the 111 to 000 position, including all the intermediate steps switching after 2 s. The displacements of the DAC and the mechAMP are recorded and analyzed by marking strategic tracking points using video analyses.

Compared to the originally simulated systems in Table 2, the displacements differ slightly, which is attributed to two aspects: First, the shift of the fabricated electrostatic actuators differs from the solid-state simulation assumption, and second, due to fabrication tolerances, the input stiffness of the mechAMPs slightly deviates. Therefore, the simulation models for Figure 13 are adapted to the experimental characterization results.

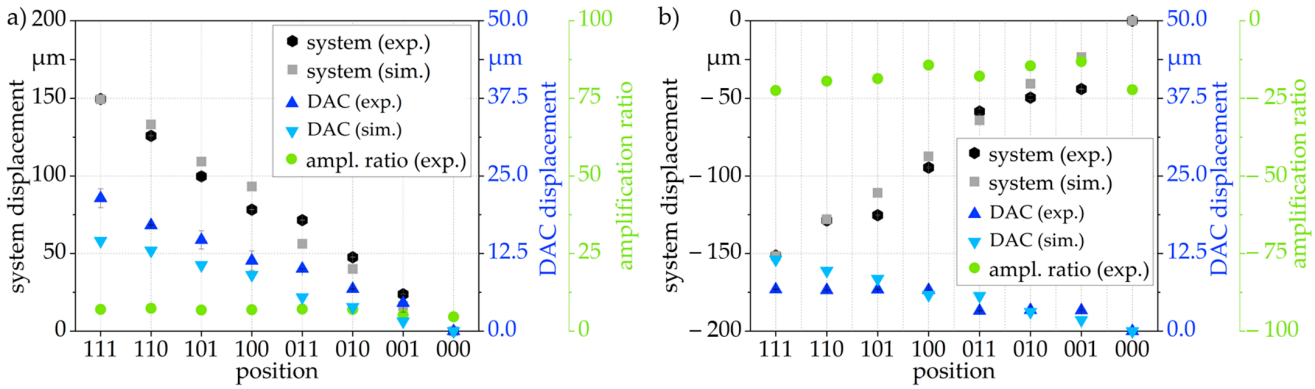

Figure 13. Simulative and experimental displacement and the resulting amplification ratio by displacing the systems in logical order from the 111 to 000 positions, including all the intermediate steps, with a switching time of 2 s for (**a**) system 1 at 60 V and (**b**) system 2 at 75 V (each experiment was repeated three times).

During the experiment, system 1 in Figure 13a shows a total stroke of 149.5 ± 0.3 µm, with an average step size of 21.4 ± 6.1 µm at the control voltage of 60 V. Compared to the simulation, the displacement shows a slight deviation at the 011 and 100 positions. The DAC reaches a total displacement of 21.4 ± 1.5 µm, with an average step size of 3.1 ± 1.1 µm. The amplification ratio calculated by Equation (3) amounts to 6.5 ± 0.9.

The mechAMP– of System 2 (Figure 13b) displaces inversely to the DAC displacement (Figure 6b). Therefore, an upwards displacement of the DAC results in a downwards displacement of mechAMP– and vice versa. Consequently, the total measured stroke at the output of mechAMP– is negative and amounts to −151.3 µm, resulting in an average step size of −21.6 ± 12.2 µm. As the variation in step size is only visible in the experimental results and does not appear during the simulation, the experimental variation is attributed to the fabrication deviations and to the high aspect ratio of the system size to displacement range. The amplification ratio of mechAMP– amounts to −16.9 ± 3.7.

4.2.4. Resonant Behavior, Switching Speed and Reliability of the System

During characterization, a minimum switching time of the bending-plate actuators between two input binary states of 0.1 ms was used successfully. The switching time of the electrostatic actuators is equal to the minimum switching speed of the device. Therefore, the minimum switching time between two input binary states is 0.1 ms, and the system can realize a frequency of up to 10 kHz. Comparing the speed of actuation to other electrostatic-actuated MEMS known from the literature, Grade et al. [17] reported an electrostatic comb-drive actuator system with approx. the same travel range as presented here of 150 µm in less than 1 ms. By characterizing a DAC based on electrostatic parallel-plate actuation, Liao et al. [6] reported a much smaller displacement of 1050 nm in less than 80 ms.

The mechanical system resonance is the limiting factor regarding the system switching frequency due to the oscillating effects. Therefore, the oscillation at the amplifier output and at the DAC was measured. System 1 was switched in logical order with all the intermediate steps from the 111 to 000 position and, finally, from the 000 to 111 position without intermediate steps. The positions were switched in 0.25-s intervals corresponding to a frequency of 4 Hz. The experiment was recorded with 4000 fps.

The oscillation amplitude of the DAC fades faster than the oscillation amplitude at the output of the mechAMP. The maximum oscillation amplitude always exceeds the step size. When switching directly from the 000 to 111 position, the system stroke has a maximum oscillation amplitude of 150.2 µm for the system and 16.6 µm for the DAC. Switching from the 100 to 011 position, the system travels the lowest displacement and exhibits a maximum oscillation amplitude of 9.5 µm for the system and of 0.3 µm for the DAC. Therefore, single-step displacement influences the oscillation amplitude. Additionally, the time until the mechAMP reaches an oscillation amplitude of less than 1 µm depends on the

displacement range. The minimum time is 0.08 s for switching from the 100 to 011 position. The maximum time is 0.2 s when switching directly from the 000 to 111 position. Therefore, depending on the required system properties, it can be useful to wait up to 0.2 s until the oscillation of the system output calms down.

The results presented in Sections 4.2.2–4.2.4 are based on experiments that were repeated three times. The deviation of the displacement of system 1 was in the range of 1.5 µm and below for a switching time of 2 s. For examining the switching speed and resonant behavior, the experiment was repeated with a faster switching speed (0.1 ms), resulting in a displacement of 149.7 µm, which is in the range of the results shown in Figure 13a (149.5 ± 0.3 µm). Therefore, a high reliability of the device operation independently from the switching speed is concluded.

4.3. High-Resolution Mode Enlarging the System Positions from $2^3 = 8$ to $3^3 = 27$

In Section 2.1, we described the system function as used in the previous sections. As announced in Section 1, a change in the electrode activation sequence allows to approach twenty-seven discrete positions with the same system. Therefore, a third stable state was added to the single bits. Initially, we only activated either the upwards or the downwards actuators and, thus, reached the known states of "1-direction" or "0-direction", as shown in Figure 14a,b. The intermediate "i-direction" (Figure 14c) is achieved by activating both the upwards and the downwards actuators simultaneously.

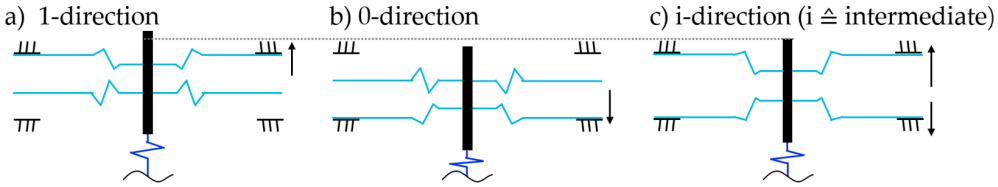

Figure 14. Bit switched to (**a**) 1-direction by activating the $a_{i,1}$ actuator, (**b**) 0-direction by activating the $a_{i,0}$ actuator and (**c**) i-(intermediate) direction by activating both the $a_{i,0}$ and the $a_{i,1}$ actuator.

The i-position does not increase the total system throw but allows to approach a larger number of defined positions and to decrease the step size. Therefore, the number of approachable positions increases from $2^3 = 8$ to $3^3 = 27$ in a 3-tri-state, with each bit having three distinct stable states. When activating the system, including the i-position, Equation (2) and its presumptions are no longer valid. Due to the controlled displacement of the actuators, the i-position is a well-defined stable position. The experimental and simulative approaches show that the actuators have to be activated to reach a well-defined multi-stable intermediate displacement. When neither the 1- nor the 0-direction actuators are activated, an intermediate position is approached by the single bit, but the system output is not defined.

The 3-tri-state activation is performed at 75 V as stiction issues appear at lower voltages due to the increased stiffness of the electrostatic actuators when activating the i-direction. The positions are switched in logical order from the 111 to 000 position, including all the intermediate steps. The experimental and simulative results presented in Figure 15 show that it is possible to realize an approximately linear stepwise displacement with the 3-tri-state system. As the system was never designed for 3-tri-state activation, slight deviations appeared during the simulation and experiment, but nonetheless, the results are promising and show a high potential to reach 27 defined positions with the originally binary eight-positions system.

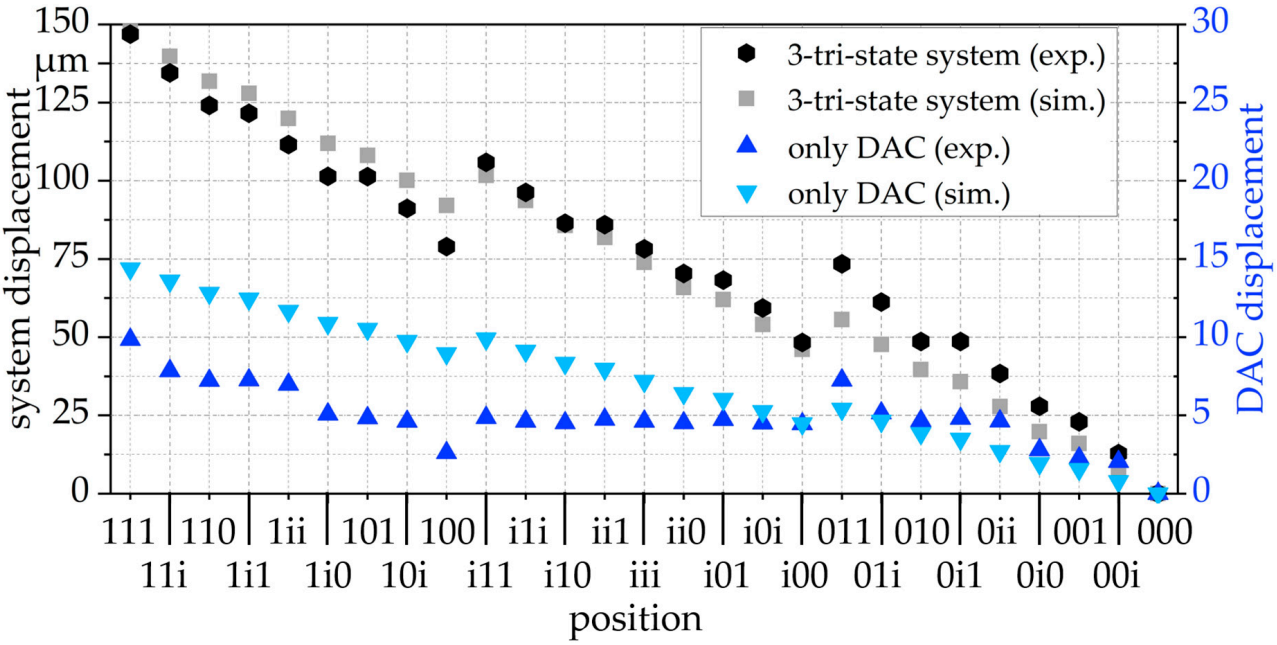

Figure 15. Experimental and simulative displacement of the DAC and the system when activating the microsystem as a 3-tri-state system at the 75-V control voltage. The positions are approached in logical order from the 111 to 000 position including the intermediate i-position (Figure 14c).

5. Conclusions

In this paper, we presented a MEMS-based electromechanical 3-bit DAC system with a maximum stepwise displacement of 149.5 µm at a voltage of 60 V within a minimum switching time of 0.1 ms. The DAC is based on multiple electrostatic bending-plate actuators connected in a parallel configuration enabling a high actuator stiffness and a low pull-in voltage at the same time. The DAC output is directly connected to a mechanical amplifier that enlarges the binary encoded DAC displacement to a large and still binary encoded system displacement.

Based on a derived system transfer function, two different systems were designed. System 1 enlarged the DAC displacement by a factor of 6.5, and System 2 enlarged and inverted the DAC displacement by a factor of −16.9. The experimental results verified the system function, the functionality of the DAC and the combined system, as well as the resonant behavior and the switching speed.

Additionally, an alternative high-resolution mode using three distinct stable states of each bit, resulting in $3^3 = 27$ discrete system positions, was found and experimentally verified. The high-resolution mode does not increase the total stroke, but it allows 27 positions instead of eight binary steps due to a different consecutive sequence of switched electrodes.

Author Contributions: Conceptualization, L.S., P.S. and M.H.; methodology, L.S.; software, L.S. and P.S.; validation, L.S.; formal analysis, L.S.; investigation, L.S.; resources, L.S., P.S. and M.H.; data curation, L.S.; writing—original draft preparation, L.S.; writing—review and editing, P.S. and M.H.; visualization, L.S.; supervision, M.H.; project administration, M.H. and funding acquisition, M.H. All authors have read and agreed to the published version of the manuscript.

Funding: This study was funded by the Deutsche Forschungsgemeinschaft (DFG, German Research Foundation)–Project-ID 287022738–TRR 196, Project C12.

Data Availability Statement: The data can be provided by the author L.S. upon reasonable request.

Acknowledgments: Some segments of the fabrication process were performed at the Center for Interface-Dominated High Performance Materials (ZGH), Ruhr University Bochum.

Conflicts of Interest: The authors declare no conflict of interest. The funders had no role in the design of the study; in the collection, analyses or interpretation of the data; in the writing of the manuscript or in the decision to publish the results.

References

1. Fu, X.; Yang, F.; Liu, C.; Wu, X.; Cui, T.J. Terahertz Beam Steering Technologies: From Phased Arrays to Field-Programmable Metasurfaces. *Adv. Opt. Mater.* **2020**, *8*, 1900628. [CrossRef]
2. Schmitt, L.; Schmitt, P.; Liu, X.; Czylwik, A.; Hoffmann, M. Micromechanical Reflect-Array for THz Radar Beam Steering based on a Mechanical D/A Converter and a Mechanical Amplifier. In Proceedings of the 2020 Third International Workshop on Mobile Terahertz Systems (IWMTS), Essen, Germany, 1–2 July 2020.
3. Liu, X.; Samfaß, L.; Kolpatzeck, K.; Häring, L.; Balzer, J.C.; Hoffmann, M.; Czylwik, A. Terahertz Beam Steering Concept Based on a MEMS-Reconfigurable Reflection Grating. *Sensors* **2020**, *20*, 2874. [CrossRef] [PubMed]
4. Sarajlic, E.; Collard, D.; Toshiyoshi, H.; Fujita, H. 12-bit microelectromechanical digital-to-analog converter of displacement: Design, fabrication and characterization. In Proceedings of the 2007 IEEE 20th International Conference on Micro Electro Mechanical Systems (MEMS), Hyogo, Japan, 21–25 January 2007.
5. Zhou, G.; Logeeswaran, V.J.; Fook, S.C. An open-loop nano-positioning micromechanical digital-to-analog converter for grating light modulation. *IEEE Photonics Technol. Lett.* **2005**, *17*, 1010–1012. [CrossRef]
6. Liao, H.-H.; Yang, Y.-J. A micromirror module using a MEMS digital-to-analog converter and its application for optical surface profiling. *J. Micromech. Microeng.* **2010**, *20*, 105009. [CrossRef]
7. Richard, Y.; Conant, R.A.; Pister, K.S.J. Mechanical digital-to-analog converters. In Proceedings of the Tenth International Solid-State Sensors and Actuators Conference, Sendai, Japan, 7–10 June 1999.
8. Liu, Q.; Huang, Q.-A. Design and finite element analysis of weighted-stiffness microelectromechanical digital-to-analogue converters. *Electron. Lett.* **2001**, *37*, 755–756. [CrossRef]
9. Pandiyan, P.; Uma, G.; Umapathy, M. Design and simulation of MEMS-based digital-to-analog converters for in-plane actuation. *Arab. J. Sci. Eng.* **2017**, *42*, 4991–5001. [CrossRef]
10. Toshiyoshi, H.; Kobayashi, D.; Mita, M.; Hashiguchi, G.; Fujita, H.; Endo, J.; Wada, Y. Microelectromechanical digital-to-analog converters of displacement for step motion actuators. *J. Microelectromech. Syst.* **2000**, *9*, 218–225. [CrossRef]
11. Non-Member, E.S.; Collard, D.; Toshiyoshi, H.; Fujita, H. Design and modeling of compliant micromechanism for mechanical digital-to-analog conversion of displacement. *IEEJ Trans. Electr. Electron. Eng.* **2007**, *2*, 357–364.
12. Schmitt, P.; Hoffmann, M. Engineering a compliant mechanical amplifier for MEMS sensor applications. *J. Microelectromech. Syst.* **2020**, *29*, 214–227. [CrossRef]
13. Martin, H.; Nüsse, D.; Voges, E. Electrostatic parallel-plate actuators with large deflections for use in optical moving-fibre switches. *J. Micromech. Microeng.* **2001**, *11*, 323.
14. Schmitt, P.; Schmitt, L.; Tsivin, N.; Hoffmann, M. Highly Selective Guiding Springs for Large Displacements in Surface MEMS. *J. Microelectromech. Syst.* **2021**, *30*, 597–611.
15. Schmitt, L.; Liu, X.; Czylwik, A.; Hoffmann, M. Design and fabrication of MEMS reflectors for THz reflect-arrays. In Proceedings of the 2021 Fourth International Workshop on Mobile Terahertz Systems (IWMTS), Duisburg, Germany, 5–7 July 2021.
16. Ibrahim, S.; Zeimpekis, I.; Kraft, M. A dicing free SOI process for MEMS devices. *Microelectron. Eng.* **2012**, *95*, 121–129.
17. Grade, J.D.; Jerman, H.; Kenny, T.W. Design of large deflection electrostatic actuators. *J. Microelectromech. Syst.* **2003**, *12*, 335–343. [CrossRef]